3D

NSC94-2212-E-216-006-

94 08 01 95 07 31

95 9 21

行政院國家科學委員會專題研究計畫成果報告

3D 視覺系統之校正與表面量測研究
A Study on the Calibration of 3D computer Vision and the Surface Measurement

摘要

　　本文使用圓形格點校正相機，使校正後的立體視覺系統具有微米量測精度。由於利用圓形格點之中心位置為校正點，且圓形格點投射於影像平面上將成橢圓形狀，因此本文使用試件圓形格點中心與影像平面橢圓中心的相關數學式，以減少相機模型方程式的偏差，此外亦於相機模型方程式中同時考慮相機之徑向與圓周向鏡頭扭曲係數，以增進相機模型方程式的精確度。相機校正之後，本文執行雙格點以及陣列格點試件之拉伸實驗，且使用立體視覺量測試件變形量，以計算軸向應變、側向應變以及浦松比等，藉此評估視覺系統量測物體變形量的精確度。

關鍵字：圓形格點、立體視覺、相機校正、鏡頭扭曲參數

Abstract

In the paper a stereo vision is calibrated using a grid of circular dots so that the calibrated system is able to measure the deformation field of a material with micron measurement accuracy. The center positions of circle dots were used as calibration points. Since the projection of a circle dot on the image plane is an ellipse, the relationship between the center of the circle dot and the center of the ellipse was obtained mathematically in the paper to reduce the bias between the camera model and the observed center of the ellipses. In addition, both of the radial and decentering lens distortions are included in the camera model equation to improve the accuracy of the model equation. After camera calibration, the tensile tests on the double-dot and dot-grid specimens were conducted and the calibrated stereo vision was used to measure the deformation field of the specimens and calculate the axial strain, lateral strain, and Poisson's ratio to evaluate the ability of the stereo vision to measure a deformed body.

Key words: circular dot, stereo vision, camera calibration, lens distortion coefficient

1. Introduction

Three-dimensional (3-D) computer vision has been widely used in the application areas like aerial imaging, robot vision, industrial metrology, and measurement of deformations in material. Hence camera calibration techniques [1] were developed to acquire the relationship between the 3-D object coordinates and the image coordinates. However, depending on the application, the requirements for the camera calibration are varied. For example, in the robot guidance application [2-4], fast and automatic calibration procedures are demanded. But in the applications to the industrial metrology and measurement of deformations in material [5-7], the accuracy of measurements, determined by the camera model and the determination of camera model parameters through calibration techniques, is a more important factor.

In general, the pinhole camera model is used to mathematically describe the imaging process [8]. To reduce the deviations from the ideal pinhole camera, radial distortion terms were added to the camera model in many researches [9,10] to produce more accurate measurement results. However, lens distortions include two components: radial distortion and decentering distortion [11]. Hence, correcting the lens distortion by only considering the radial effect is not sufficient for modeling the mapping precisely. The addition of decentering terms appears necessary [12].

Based on the digital image correlation (DIC) [13,14], Luo et al [6,7] developed a 3-D vision system to successfully conduct the researches on curved surface measurements [15,16] and fracture mechanics [17-19]. In the system, only accounted for is the radial distortion coefficient and N calibration points in space are obtained by moving a calibration target mounted in a three axis translation stage N times. While the two dimensional deformation field of an object can be accurately measured, the calibration procedure is tedious and time consuming. In recent, Luo and Wu [20,21] used a grid of circular dots to make the calibration work speed up and satisfactory results were obtained. While the center of the ellipse, formed by the projection of a circular dot in the space into an image plane, is determined using Bookstein's

method [22], the relationship between the center positions of the circle and the ellipse is not described mathematically. Therefore, the measurement accuracy of the developed system is limited.

In the paper a dot target, a translation stage, and a CCD camera with its sensor plane being parallel to the surface of the dot target were used to determined the center position of the circular dots on the dot target so that a world coordinate system and M calibration points can be obtained. Then these M calibration points were used to calibrate the stereo vision formed by two CCD cameras. Since the projection of the circle dot on the image plane is an ellipse [23], the relationship [12] between the center of the circle dot and the center of the ellipse was obtained mathematically in the paper to reduce the bias between the camera model and the observed center of the ellipses. In addition, both of the radial and decentering lens distortions are included in the camera model to improve the accuracy of the model equation.

After camera calibration, the tensile tests on the double dots specimen, the dot grids specimen, and the random pattern specimen were conducted and the calibrated stereo vision was used to measure the deformation field of the specimens and calculate the axial strain, lateral strain, and Poisson's ratio to evaluate the ability of the stereo vision to measure a deformed body.
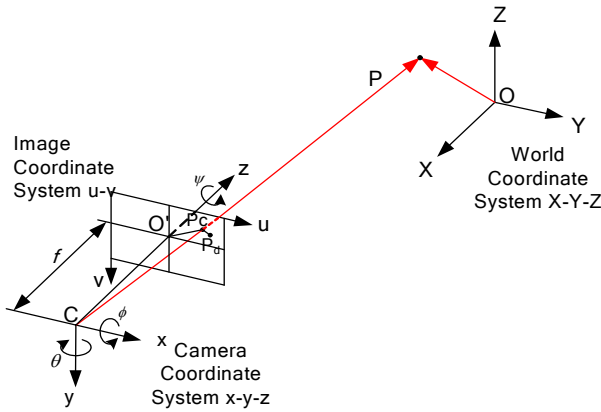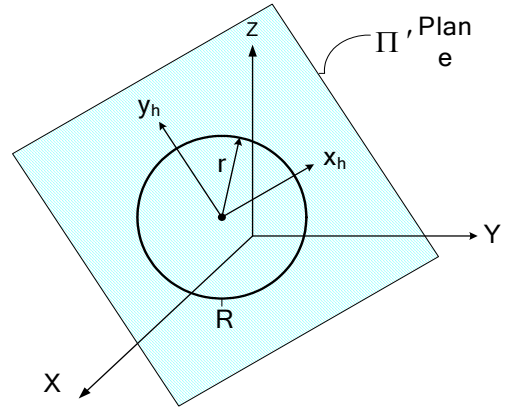

Figure 1 Camera model with lens distortion

Figure 2 Circle on a plane

2. Camera Model

As shown in Figure 1, the image plane is in front of the lens center C and the focal length f is the distance between the image plane and the lens center; O and O′ are the centers of the world coordinate system X-Y-Z and the image coordinate system u-v, respectively; C is the center of the camera coordinate system x-y-z. The u- and v-axes are parallel to the x- and y-axes, respectively. The projection of the object point $P(X, Y, Z)$ in world coordinates to the image point $P_c(u_c, v_c)$ in image coordinates can be ideally described by the following equation

$$\begin{bmatrix} zu_c \\ zv_c \\ z \end{bmatrix} = F \begin{bmatrix} X \\ Y \\ Z \\ 1 \end{bmatrix},$$

(1)

where $\mathbf{F}$ is a perspective transformation matrix which is defined by focal length f, image plane center (u_0, v_0), translation vector $\mathbf{t} = [t_x, t_y, t_z]$ between the world and camera frames, and rotation matrix $\mathbf{R} = \mathbf{R}(\theta, \phi, \varphi)$. It is noted that θ, ϕ, and φ are the angles of rotation about the y, x, and z axes, respectively. In practice, radial distortion and decentering effects are present in most lenses. The corrections (Δu, Δv) are added to the distorted image coordinates (u_d, v_d) to get the corrected image coordinates (u_c, v_c): [12]

$$\begin{bmatrix} u_c \\ v_c \end{bmatrix} = \begin{bmatrix} u_d \\ v_d \end{bmatrix} + \begin{bmatrix} \Delta u(u_d, v_d) \\ \Delta v(u_d, v_d) \end{bmatrix}.$$

(2)

In eq (2), (Δu, Δv) are defined by the coefficients for the radial distortion (k_1, k_2) and the coefficients for the decentering (p_1, p_2). Eq (2) may be rewritten as [12]

$$\begin{bmatrix} u_d \\ v_d \end{bmatrix} \approx \begin{bmatrix} u_c \\ v_c \end{bmatrix} - \frac{1}{d} \begin{bmatrix} \Delta u(u_c, v_c) \\ \Delta v(u_c, v_c) \end{bmatrix},$$

(3)

where $d = 4k_1r_c^2 + 6k_2r_c^4 + 8p_1(v_c - v_0) + 8p_2(u_c - u_0) + 1$.

Using eqs (1) and (3), a forward camera model is obtained to map an object point P in world coordinates to a distorted image point P_d in image coordinates. However, using a backward camera model formed by eqs (2) and (1), the location of an object point is not determined uniquely by its image point.

3. Center of Circular Dots

As shown in Figure 2, a circle with radius r is located on the Π' plane so that its center $h_0(X_0, Y_0, Z_0)$ is the origin of the planar coordinate system x_h-y_h. Under the world coordinate system X-Y-Z, the direction cosines of the axes x_h and y_h are $\mathbf{h_1} = (X_1, Y_1, Z_1)$ and $\mathbf{h_2} = (X_2, Y_2, Z_2)$, respectively. Referenced to the x_h-y_h coordinate system, the circle equation may be expressed as

$$\begin{bmatrix} x_h \\ y_h \\ 1 \end{bmatrix}^T \begin{bmatrix} -1/r^2 & 0 & 0 \\ 0 & -1/r^2 & 0 \\ 0 & 0 & 1 \end{bmatrix} \begin{bmatrix} x_h \\ y_h \\ 1 \end{bmatrix} = \begin{bmatrix} x_h \\ y_h \\ 1 \end{bmatrix}^T Q \begin{bmatrix} x_h \\ y_h \\ 1 \end{bmatrix} = 0, \tag{4}$$

Using eq (1), the circle can be projected on the image plane. The resulted curve will be an ellipse or a circle and may be expressed as

$$\begin{bmatrix} zu_c \\ zv_c \\ z \end{bmatrix}^T ((FH)^{-1})^T Q (FH)^{-1} \begin{bmatrix} zu_c \\ zv_c \\ z \end{bmatrix} = 0, \tag{5}$$

where $H = \begin{bmatrix} h_1 & h_2 & h_0 \\ 0 & 0 & 1 \end{bmatrix}$.

The center (u_e, v_e), expressed in the planar coordinate system x_h-y_h, of the ellipse may then be obtained by [23]

$$\lambda \begin{bmatrix} u_e \\ v_e \\ 1 \end{bmatrix} = F(HQ^{-1}H^T)F^T \begin{bmatrix} 0 \\ 0 \\ 1 \end{bmatrix}. \tag{6}$$

Using eq (3), the center (u_e, v_e) of the resulted ellipse can be converted to the distorted coordinates (u, v) by

$$\begin{aligned} u &= M_x(u_e + \Delta u) \\ v &= M_y(v_e + \Delta v) \end{aligned}, \tag{7}$$

where M_x and M_y represent conversion factors that specify the relationship between pixels and the physical object units. Eqs (6) and (7) relate the center of a circle in space to the distorted image point on an image plane by using the 15 camera parameters M_x, M_y, f, k_1, k_2, p_1, p_2, (u_0, v_0), (t_x, t_y, t_z), and (θ, ϕ, φ).

4. Experiments

4.1 Camera calibration

Figures 3 and 4 show the configuration of the 3-D measurement system and the schematic illustration of the experimental setup for the calibration experiments, respectively. It is noted that the dot target is placed on the MTS machine and the measurement system is put on a separate work station to prevent the system from being influenced by the vibration of the MTS machine when a tensile test is performed. As indicated in Figure 5, the dot target with an N by N array of circular dots was mounted on a translation stage and used to calibrate the stereo vision formed by camera one and two having nearly the same pan angle and viewing the same area of an object. In the paper the CCD camera (JAI CVM1) equipped with a 8.9 by 6.7 mm sensor area and a 55 mm lense (Nikkor), the frame grabber (Matrox Meteor II), and the Pentium PC formed a stereo vision system to acquire a pair of image of an object. The size of the image is 1280 by 1024 pixels.
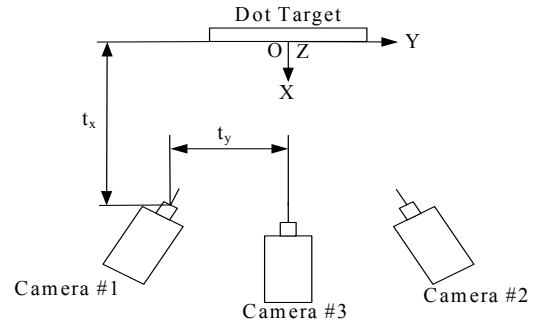
Figure 3 Experimental setup for camera calibration

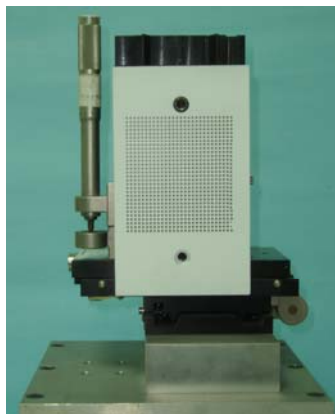Figure 4 Top view of experimental setup for calibration test

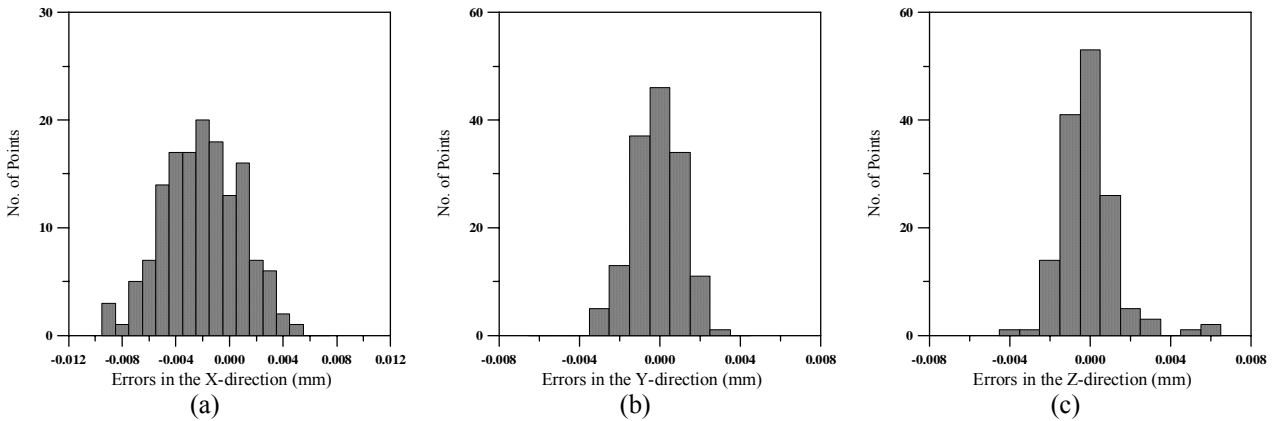Figure 5 Dot target mounted on a XYZ translation stage

(a)

(b)

(c)

Figure 6 Error distribution for measured calibration points in the X-, Y-, and Z-directions

As in previous work [20,21], the dot target and camera three shown in the Fig. 4 form a grid calibration system and are used to accurately calibrate the location of the dots relative to an erected object coordinate system Y-Z. It is noted here that in the setup of the 3-D measurement system the sensor area of camera three is almost parallel to the surface of the dot target, i.e., the sensor area is perpendicular to the x-direction of the translation stage. The grid image with a resolution of 640 by 480 pixels was captured using a JAI CVM10 CCD camera equipped with a 105 mm Nikkor lens. It is noted that in the paper the dot center is taken as calibration point. Following the determination of the location of the N by N circular dots, a world coordinate system X-Y-Z and M calibration points with known world coordinates were then resulted. It is also noted that the X-axis is sensed in the X-direction of the translation stage. With these calibration points in the space and their corresponding conjugate pairs (i.e., the projections of the calibration points onto the image planes of camera one and two), each camera in the stereo vision system was calibrated independently using the

4

Levenberg-Marquardt method [24] to extract the fifteen camera parameters. For detailed procedures of camera calibration used in the paper, refer to [20] and [21]. Presented in Table 1 are the determined camera parameters.

Using the calibrated camera parameters and the known conjugate pairs, the measured calibration points were obtained. The errors of the calibration points were then evaluated by subtracting the measured calibration points from the known calibration points. Figure 6 shows the error distribution for measured calibration points in the X-, Y-, and Z-directions and indicates that the error distribution follows the shape of a normal distribution. From the examination of Fig. 6, it is also noted that for the error distributions in the Y- and Z-directions, the sample mean appears to occur near the middle of the data where the errors are concentrated. Similar results were observed for other calibration experiments.
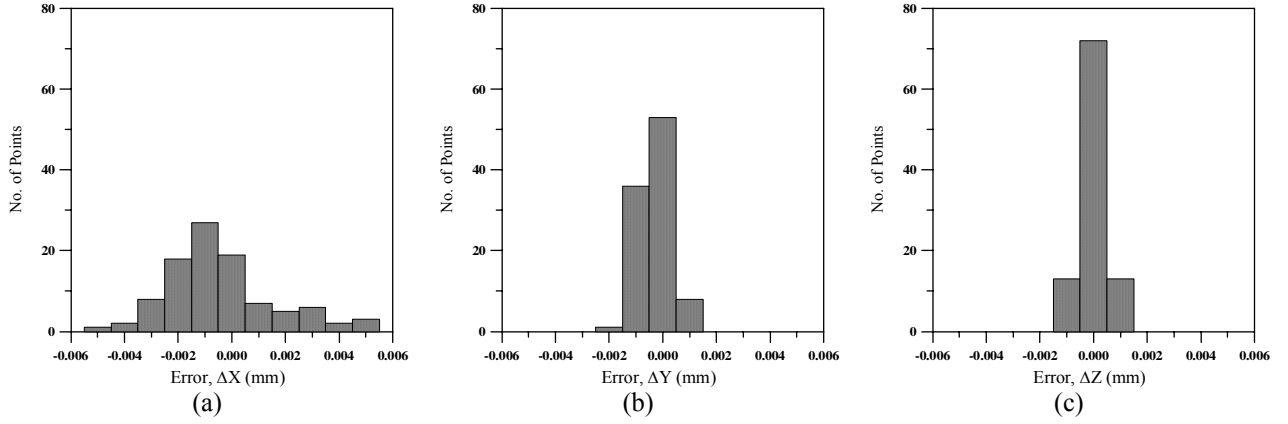
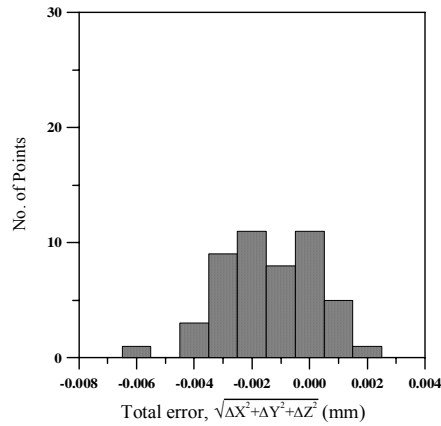Figure 7 Error distribution for the out-of-plane-displacement test

Figure 8 Error distribution for the 3-D displacement test

4.2 *Rigid body translation tests*

After the camera calibration, rigid body translations were performed to evaluate the measurement accuracy of the stereo vision. First, the target was displaced with a specific amount relative to the world coordinate system and the calibrated stereo vision was used to acquire the gird image before and after the translation. The conjugate pairs corresponding to the N by N grid's circles were obtained using Bookstein's method and the location of these N by N circular points relative to the world coordinate system, before and after the translation, was then obtained using the determined camera parameters and the camera model equations (7), (2), and (1). The displacement of these circular points was computed and compared to the known amount of displacement to analyze the measurement error.

Shown in Figures 7 and 8 are the frequency distribution for the displacement measurement error of the 7 by 7 grid circles displaced $(1,0,0)$ mm and $(1,1,1)$ mm relative to the world coordinate system, respectively. Fig. 7 indicates that while the sample mean for the in-plane-displacement measurement errors ΔY and ΔZ approaches to zero, the sample mean for the out-of-plane-displacement measurement error ΔX approaches to -0.001 mm. It is also observed from Fig. 7 that the distribution for the measurement error ΔX is more disperse than those for the measurement errors ΔY and ΔZ. Since the Y- and Z-axes of the erected world coordinate system may be not aligned with the y- and z-axes of the translation stage, Fig. 8 only shows the frequency distribution for the total displacement measurement error $\sqrt{\Delta X^2 + \Delta Y^2 + \Delta Z^2}$. It is found that most of the total errors occur between -0.003 mm and 0.001 mm.

4.3 *Tensile tests*

In the paper the tension test specimens were made of Aluminum 5052. White paint was first sprayed onto the surface of the specimen and then circle grid was pasted on its surface to make a pattern of double dots or circle grid. Also white and black paint was sprayed onto the surface of the specimen to produce a random pattern. Tensile tests were conducted on these specimens and the calibrated stereo vision was used to measure their deformation field. The axial and lateral strains were measured simultaneously to obtain the stress-strain curve and Poisson's ratio of the Aluminum 5052 to evaluate the ability of the stereo vision to measure a deformed body. It is noted that in the experiments a load cell and an extensometer with the extended gage length of 25 mm were used to record the applied load and the elongation of the specimens, respectively.
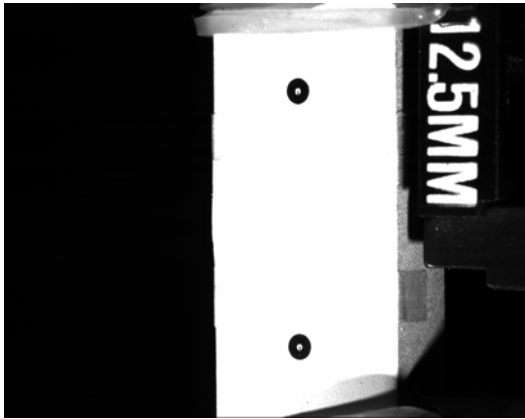

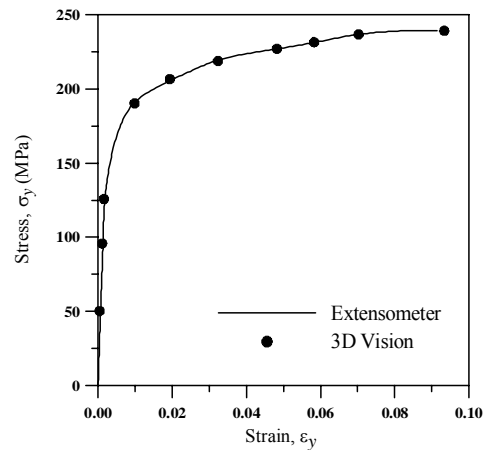Figure 9 Image of double-dot specimen taken by camera two at the applied load of 21.9 kN

Figure 10 Stress-strain curve for AL 5052 (double-dot specimen)

Shown in Figure 9 is the image of the tension test specimen with the pattern of double dots taken by camera two at the applied load of 21.9 kN. By processing the images before and after the deformation of the specimen, the center position of both dots is determined and the axial strain of the specimen is obtained by $\varepsilon_y = \Delta l / l_0$, where l_0 is the original distance between the dots and Δl the change of the distance. The stress-strain curve of the AL 5052 is shown in Figure 10. Results indicate that the obtained axial strains are in good agreement with the strain measurements of the extensometer.

Figure 11 shows the image of the tension test specimen with a grid of circular dots. By measuring the center position of the top and bottom dots located at the 2nd or 3rd column of the grid before and after the deformation of the specimen, the axial strain was computed using $\varepsilon_y = (\Delta l / l_0)_y$. In a similar way, the lateral strain was computed using $\varepsilon_x = (\Delta l / l_0)_x$ by measuring the center position of the left and right dots located at the 4th or 5th row of the grid. As indicated in Table 2, the computed values of ε_x and ε_y were compared to the extensometer measurements at several applied loads. Poisson's ratio calculated by $(\Delta l / l_0)_x / (\Delta l / l_0)_y$ is also presented in Table 2. A larger deviation between the axial strain measurements of the extensometer and stereo vision is found at the small strain values of 0.05 percent. This large deviation is due to fact that the measurement accuracy of the 3-D measurement system is about ± 100 micro-strains. For larger axial strain values, it is observed that the deviation is within the range of 0.9 percent to 7.9 percent. At the strain value of 0.02 percent, in which the material is in the elastic deformation state, the calculated Poisson's ratio is 0.343. When the axial strain value is increased to 0.43 percent or higher, the material starts to enter the plastic deformation state and the measured Poisson's ratio approaches to 0.399.
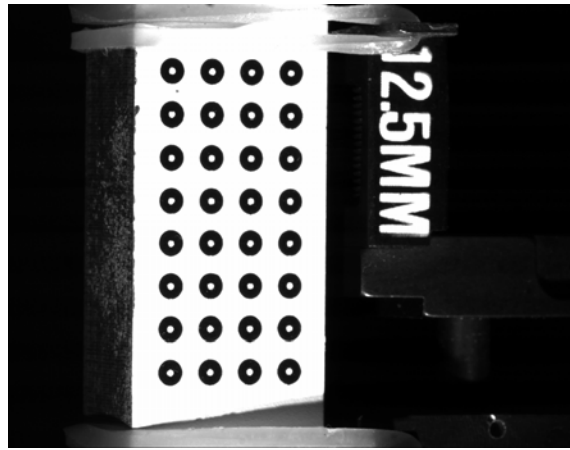
Figure 11 Image of dot-grid specimen taken by camera one at the applied load of 16.0 kN

Shown in Figure 12 is the image of the tension test specimen with a random pattern, which was taken by camera one. In this image a 31 × 31 rectangular array of points was selected within the central region of the specimen to find, by using DIC [13,14], their corresponding points in the image plane of camera two. Using the determined conjugate image pairs and camera parameters, the position of the grid points can be obtained [6,7] relative to an object coordinate system x-y, whose origin is located at the center point of the selected rectangular array. The displacement field of the specimen was obtained using the determined position of the grid points before and after the deformation of the specimen. A smoothing technique was then used to smooth the displacement field to determine the in-plane strains ε_x, ε_y and ε_{xy} of the specimen. The resulted stress-strain curve shown in Figure 13 is similar to that obtained from the double-dot test specimen. The strain measurements for the aluminum 5052 specimen are summarized in Table 3. It is found from Table 3 that the computed axial strains appear to be in good agreement with the extensometer measurements. Most of the mean errors of the computed shear strain are below 100 micro-strains. When the axial strain value is increased to 0.36 percent or higher, the mean error is increased to about 200 micro-strains. At the axial strain value of 0.07 percent, in which the material is in the elastic deformation state, the calculated Poisson's ratio is 0.334. However, for the material being in the plastic deformation state, the measured Poisson's ratio approaches to 0.466.
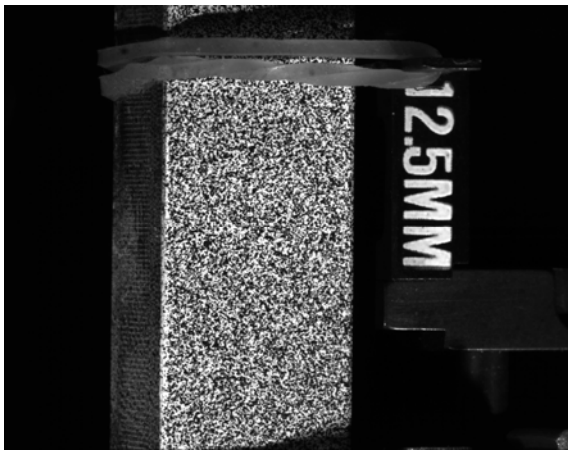

Figure 12 Image of random-patterm specimen taken by camera one at the applied load of 4.96 kN
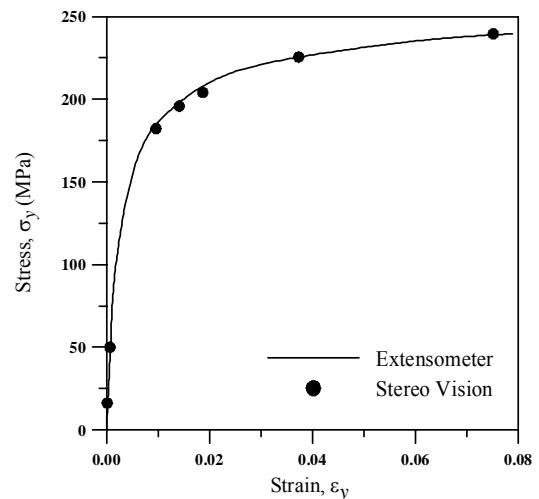
Figure 13 Stress-strain curve (random-pattern specimen)

5. Conclusions

The 3-D measurement system described in this paper is composed of two parts: (a) stereo vision system and (b) grid calibration system. The grid calibration system is used to accurately determine the spacing of the circle grid so that the stereo vision can be calibrated more precisely. Since the projection of a circular dot onto the image plane is an ellipse, the relationship between the center of the circular dot and the center of the ellipse is obtained mathematically to reduce the bias between the camera model and the observed center of the ellipses. In addition, both radial and decentering lens distortions are included in the camera model to increase the accuracy of the model equation. The proposed 3-D measurement system was calibrated successfully and an approximate error of ±1 μm for each displacement component

7

was obtained from (1,0,0) mm rigid body translation tests. For (1,1,1) mm rigid body translation tests, the total error is about ±2 μm. Experimental results for the tensile tests conducted in the paper indicate that the 3-D measurement system can be applied to measure a deformation field of a deformed object. The 3-D measurement system has the advantage that the accuracy of the measured in-plane displacement components will be not affected by the out-of-plane motion of the object. The measurement accuracy of the proposed system may be improved by using a high precision translation stage and a commercial dot target.

References

1. Abdel-Aziz, Y. I. and Karara H.M., "Direct Linear Transformation into Object Space Coordinates in Close-Range Photogrammetry," *Proc. Symp. Close-Range Photogrammetry*, 1-18, Jan. 1971.
2. Tsai, R., "A versatile camera calibration technique for high-accuracy 3D machine vision metrology using off-the-shelf TV camera and lenses", *IEEE Trans, Robotics and Automation*, 3(4) (1987).
3. Ganapathy, S., "Decomposition of Transformation Matrices for Robot Vision," *Pattern Recognition Letters*, 2, 401-142 (1984).
4. Faugeras, O. D. and Toscani, G., "Camera Calibration for 3D Computer Vision," *Proceeding of International Workshop Industrial Application of Machine Vision and Machine Intelligence*, 240-247, Feb. 1987.
5. Carbon, V., Carocci, M., Savio, E., Sansoni, G., and Chiffre, L. D., "Combination of Vision System and a Coordinate Measuring Machine for the Reverse Engineering of Freeform Surfaces," *Advanced Manufacturing Technology*, 17, 263-271 (2001).
6. Luo, P. F., Chao, Y. J., Sutton, M. A. and Peters. W. H., "Accurate Measurement of three-dimensional Deformations in Deformable and Rigid Bodies Using Computer Vision", *Experimental Mechanics*, 33(2), 123-132 (1993).
7. Luo, P. F., Chao, Y.J., and Sutton, M. A., "Application of Stereo Vision to Three-dimensional Deformation Analyses in Fracture Experiments, "*Optical Engineering*, 33(3), 981-990 (1994).
8. Faugeras, O., *Three-dimensional Computer Vision*: A Geometric View Point, MIT Press, Cambridge, MA (1993).
9. Beyer, N. A., "Accurate Calibration of CCD Cameras," *in Conference on Computer Vision and Pattern Recognition* (1992).
10. Weng, J, Cohen, P., and Herniou, M., "Camera Calibration with Distortion Models and Accuracy Evaluation", *IEEE Transaction on Pattern Analysis and Machine Intelligence*, 14(10), 965-980 (1992).
11. Manual of Photogrammetry, fourth ed., Slama, C.C., ed., Falls Church, Va,, *American Society for Photogrammetry*, 1980.
12. Heikkila, J., "Geometric Camera Calibration Using Circular Control Points," *IEEE Transaction on Pattern Analysis and Machine Intelligence*, vol. 22, No. 10, October (2000).
13. Sutton, M. A., Wolters, W. J., Peters, W. H., Ranson, W. F. and McNeill, S. R., "Determination of Displacements Using an Improved Digital Correlation Method," *Image and Vision Computing*, 1 (3), 133-139 (1983).
14. Chu, T. C., Ranson, W. F., Sutton, M. A. and Peters, W. H., "Applications of Digital Image Correlation Techniques to Experimental Mechanics," *Experimental Mechanics*, 25(3), 232-244 (1985).
15. Luo, P. F. and Liou, S. S., "Measurement of Curved Surface by Stereo Vision and Error Analysis," *Optics and Lasers in Engineering*, 30(6), 471-486 (1998).
16. Luo, P. F. and Chen, J. N., "Measurement of Curved Surface Deformation in Cylindrical Coordinates," *Experimental Mechanics*, 40(4), 345-350 (2000).
17. Luo, P. F. and Huang, F. C., "Application of stereo Vision to the Study of Mixed-mode Crack-tip Deformations," *Optics and Lasers in Engineering*, 33(5), 349-368 (2000).
18. Luo, P. F. and Huang, F. C., "An Experimental Study on the Mixed-mode Crack-tip Deformations in PMMA," *Journal of Strain Analysis for Engineering Design*, 38(4), 313-318 (2003).
19. Luo, P. F., Chuang, C. K., and Chao, Y. J., "Measurement of J Integral by Shadow Spot Generated from Out-of-plane Displacement," *Optical Engineering*, 42(12), 3433-3442 (2003).
20. Luo, P. F. amd Wu J., "Camera Calibration and Three-dimensional Deformation Measurements Using Circle Grid," Proceedings of the 2004 SEM X International Congress and Exposition on Experimental and Applied Mechanics, Costa Mesa, California, USA.
21. Wu, J., *An experimental Study on the Application of a Grid of Circular Dots to Camera Calibration*, Master thesis, Chung Hua University (2002).
22. Bookstein, F. L., "Fitting Conic Sections to Scattered Data," *Computer Grapics and Image Processing*, 9, 56-71 (1979).
23. K. Kanatani, *Geometric Computation for Machine Vision*. Oxford: Clarendon Press, 1993.
24. Press, W. H., Teukolsy, S. A., Vetterling, W. T., and Flannery, B. P., *Numerical Recipes in C—The Art of Scientific Computing*, second ed., Cambridge University Press, 1992.
25. Jain, R., Kasturi, R. and Schunck, B. G., Machine Vision, McGraw-Hill International Editions, 382-383 (1995).

Camera Parameters	Unit	Camera #1		Camera #2	
		Guessed Initial Values	Predicted Values	Guessed Initial Values	Predicted Values
f	mm	74.	64.466	74.0	70.379
k_1	10^{-3}mm^{-2}	0.01	0.0596	0.01	0.0444
k_2	10^{-5}mm^{-4}	0.01	-0.469	0.01	-0.0484
p_1	10^{-4}mm^{-1}	1.0	1.94	1.0	1.01
p_2	10^{-4}mm^{-1}	1.0	-1.11	1.0	-1.03
M_x	Pixel/mm	147.0	164.445	147.0	149.666
M_y	Pixel/mm	148.0	162.787	148.0	150.831
h_0	mm	4.35	3.892	4.35	4.274
v_0	mm	3.45	3.159	3.45	3.410
θ	degree	25.0	24.494	-25.0	-25.431
ϕ	degree	0.0	1.626	0.0	1.020
φ	degree	0.0	-0.230	0.0	0.812
t_x	mm	245.0	245.883	245.0	242.265
t_y	mm	-110.0	-103.614	110.0	121.198
t_z	mm	0.0	2.867	0.0	2.304

Table 1 camera parameters

Applied Load (kN)	Extensometer Measurements ($\times10^{-6}$)	Stereo Vision Measurements ($\times10^{-6}$)			$\nu = -\dfrac{(\Delta l/l_0)_x}{(\Delta l/l_0)_y}$
		$\varepsilon_y = (\Delta l/l_0)_y$	Percentage Error	$\varepsilon_x = (\Delta l/l_0)_x$	
6.3	552	417	24.4	-128	0.307
161	2006	2041	1.7	-701	0.343
19.9	4304	4645	7.9	-1657	0.357
22.0	12279	12451	1.4	-4725	0.379
23.6	24525	24759	0.9	-9551	0.386
24.1	29926	30998	3.6	-12285	0.396
25.3	46376	47816	3.1	-18949	0.396
25.8	58626	59175	0.9	-23441	0.396
26.0	73839	75417	2.1	-30081	0.399

Table 2 Strain measurements for the AL 5052 tension test specimen at several applied loads (circle-grid specimen)

Applied Load (kN)	Extensometer Measurements ($\times 10^{-6}$)	Stereo Vision Measurements ($\times 10^{-6}$)							$\nu = -\dfrac{\varepsilon_{xx}}{\varepsilon_{yy}}$
		$\varepsilon_{yy} = \dfrac{\partial v}{\partial y}$		$\varepsilon_{xx} = \dfrac{\partial v}{\partial y}$		$\varepsilon_{xy} = \dfrac{1}{2}\left(\dfrac{\partial u}{\partial y} + \dfrac{\partial v}{\partial x}\right)$			
		Mean Value	Standard Deviation	Mean Value	Standard Deviation	Mean Value	Standard Deviation	Poisson's ratio
1.6	176	150	46	-45	26	-25	22	0.300
5.0	732	694	121	-232	20	-35	44	0.334
18.2	8980	9636	84	-4208	65	-34	78	0.437
19.6	13245	14133	56	-6235	56	9	34	0.441
20.4	17773	18688	264	-8381	86	-87	101	0.448
22.6	36285	37323	267	-16947	358	-123	148	0.454
24.0	78843	75112	882	-35037	558	-247	196	0.466

Table 3 Strain measurements for the AL 5052 tension test specimen at several applied loads (random pattern specimen)

計畫成果自評

　　本計畫之研究內容與原計畫之相符程度約為 80%，並已達成下列之原計畫預期目標：

1. 使用試件圓形格點中心與影像平面橢圓形中心的數學關係式，以減少相機模型方程式的偏差，同時亦將考慮切向的鏡頭扭曲係數，以增近相機模型方程式的精確度。
2. 利用平台系統、格點校正試件以及一台光軸垂直於校正試件的相機，精確求取校正試件上各格點的座標位置，以建立世界座標系統以及 M 個校正點的座標位置。
3. 藉 M 個校正點，校正兩台各平掃某一角度的 CCD 相機所形成的 3D 視覺系統。
4. 進行剛體平移測試，來驗證本計畫所提 3D 視覺系統的精度與可靠度。
5. 本計畫所提的 3D 視覺系統，於校正後，可量測物件之三維尺寸以及變形物體的三維變形場。

由於時間所限，本研究係以手動方式控制移動平台，並未進行整合 3D 視覺系統、雷射干涉儀量測系統以及平台控制，以建立完全自動校正之軟硬體設施。但本研究成果除可在諸如 Optical Engineering 等光學領域的學術期刊發表外，並可作為 3D 視覺系統校正與量測之重要參考。

可供推廣之研發成果資料表

□ 可申請專利　　■ 可技術移轉　　　　　　　　　日期：<u>95</u>年<u>9</u>月<u>14</u>日

國科會補助計畫	計畫名稱：3D 視覺系統之校正與表面量測研究 計畫主持人：羅鵬飛 計畫編號：NSC 94-2212-E-216-006　　　學門領域：精密量測
技術/創作名稱	3D 視覺量測系統
發明人/創作人	羅鵬飛
技術說明	中文： 本文使用圓形格點校正相機，使校正後的立體視覺系統具有微米量測精度。由於利用圓形格點之中心位置為校正點，且圓形格點投射於影像平面上將成橢圓形狀，因此本文使用試件圓形格點中心與影像平面橢圓中心的相關數學式，以減少相機模型方程式的偏差，此外亦於相機模型方程式中同時考慮相機之徑向與圓周向鏡頭扭曲係數，以增進相機模型方程式的精確度。 英文： In the paper a stereo vision is calibrated using a grid of circular dots so that the calibrated system is able to measure the deformation field of a material with micron measurement accuracy. The center positions of circle dots were used as calibration points. Since the projection of a circle dot on the image plane is an ellipse, the relationship between the center of the circle dot and the center of the ellipse was obtained mathematically in the paper to reduce the bias between the camera model and the observed center of the ellipses. In addition, both of the radial and decentering lens distortions are included in the camera model equation to improve the accuracy of the model equation.
可利用之產業 及 可開發之產品	可應用於機器人視覺、工業量測以及材料變形量測等各種不同領域。
技術特點	使用試件圓形格點中心與影像平面橢圓形中心的數學關係式，以減少相機模型方程式的偏差，同時亦將考慮切向的鏡頭扭曲係數，以增近相機模型方程式的精確度。利用平台系統、格點校正試件以及一台光軸垂直於校正試件的相機，精確求取校正試件上各格點的座標位置，以建立世界座標系統以及 M 個校正點的座標位置。
推廣及運用的價值	可協助業界開發 3D 視覺檢測平台。